The Pennsylvania State University

Hurricane Katrina

A Land Cover Change Detection Analysis Spanning 15 Years

MGIS Capstone

ABSTRACT

On August 29, 2005, Hurricane Katrina made landfall as a category three storm in southeast Louisiana, with maximum wind speeds of 110 knots. This study analyzes Landsat imagery from three distinct time-periods over Southeast Louisiana. One from 2003, prior to the hurricane; another from 2005, shortly after the hurricane; and finally from 2020, 15 years after the hurricane devastated the area. This study used a random forest (RF) land cover classification (LCC) methodology within Google Earth Engine (GEE) in order to assess changes in land cover as well as recovery. Additionally, this study uses Normalized Difference Vegetation Index (NDVI) to assess changes in vegetation health throughout the three time-periods. These land cover change detection metrics indicate a loss of wetlands, and NDVI indicates a drastic decrease in vegetation health from 2003 to 2005. From 2003 to 2020, there is a notable decrease in NDVI and a continued loss of wetland area since Hurricane Katrina. This is an urgent matter due to the devastating effect this vegetation loss has on local ecology, including the many threatened and endangered wildlife and marine species that call this area home.

Additional Index Words: NDVI, Wetlands, Random Forest, Google Earth Engine

I. INTRODUCTION

Hurricane Katrina is one of the most catastrophic natural disasters in all United States history [Knabb *et al.,* 2005]. On August 29, 2005, Hurricane Katrina made landfall as a category three storm in southeast Louisiana, with maximum wind speeds of 110 knots [NCDC, 2005]. This makes Hurricane Katrina a major hurricane according to the Saffir-Simpson Hurricane Wind Scale. Although the hurricane weakened to a Category 3 prior to landfall, it still carried with it much of the storm surge it had built as a Category 5 in the Gulf of Mexico, with inundation reaching 30 feet in some areas [NCDC, 2005]. The estimated cost of damage from the hurricane is $125 billion dollars [NCDC, 2005]. Tropical cyclones, "are one of the most common natural drivers of coastal disturbance and widespread morphological change," and major hurricanes like Hurricane Katrina, "cause the most observable wetland loss" [Morton and Barras, 2011]. False color composite images from October 4, 2003 and October 25, 2005 help to visualize the obvious changes to the wetland composition in the area (Figure 1). This false color composite uses the near infrared band displayed with the red image plane so that healthy vegetation appears red. The image on the left is from October 4, 2003, prior to hurricane landfall, and the image on the right is from October 25, 2005, two months after hurricane landfall. There is a significant reduction of redness in the image captured after landfall, and increased area of water, indicating decreased vegetation health or total loss of vegetation.

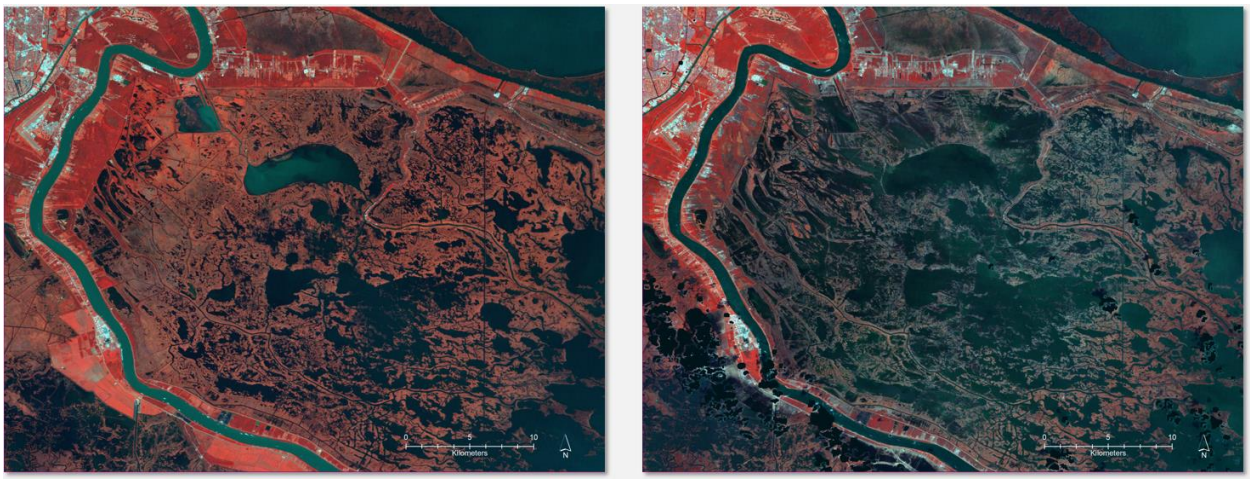

Figure 1. Before and after false color composite Landsat images: October 4, 2003 (left) and October 25, 2005 (right).

Wetlands have high levels of biodiversity and are a major source of carbon sequestration [Wright & Gallant, 2007]. The Mississippi River delta specifically is a home for numerous endangered and threatened animal species, [www.nwf.org]. Wetlands are not only important for biodiversity and carbon sequestration but are also valuable for reducing the damaging effects of hurricanes on coastal communities [Costanza *et al.,* 2008].

Hurricane Katrina moved directly north over the Mississippi River Delta region, putting much of the wetland area in the most intense part of the eye wall, the northern section (Figure 2). One study puts the value of the storm protection lost from Hurricane Katrina's wetland destruction at USD 1.1 billion [Costanza *et al.,* 2008]. For this reason, it is important to study the rebound of the coastal wetlands that were lost due to Hurricane Katrina, and to explore ways to decrease hurricane impacts on coastal communities.

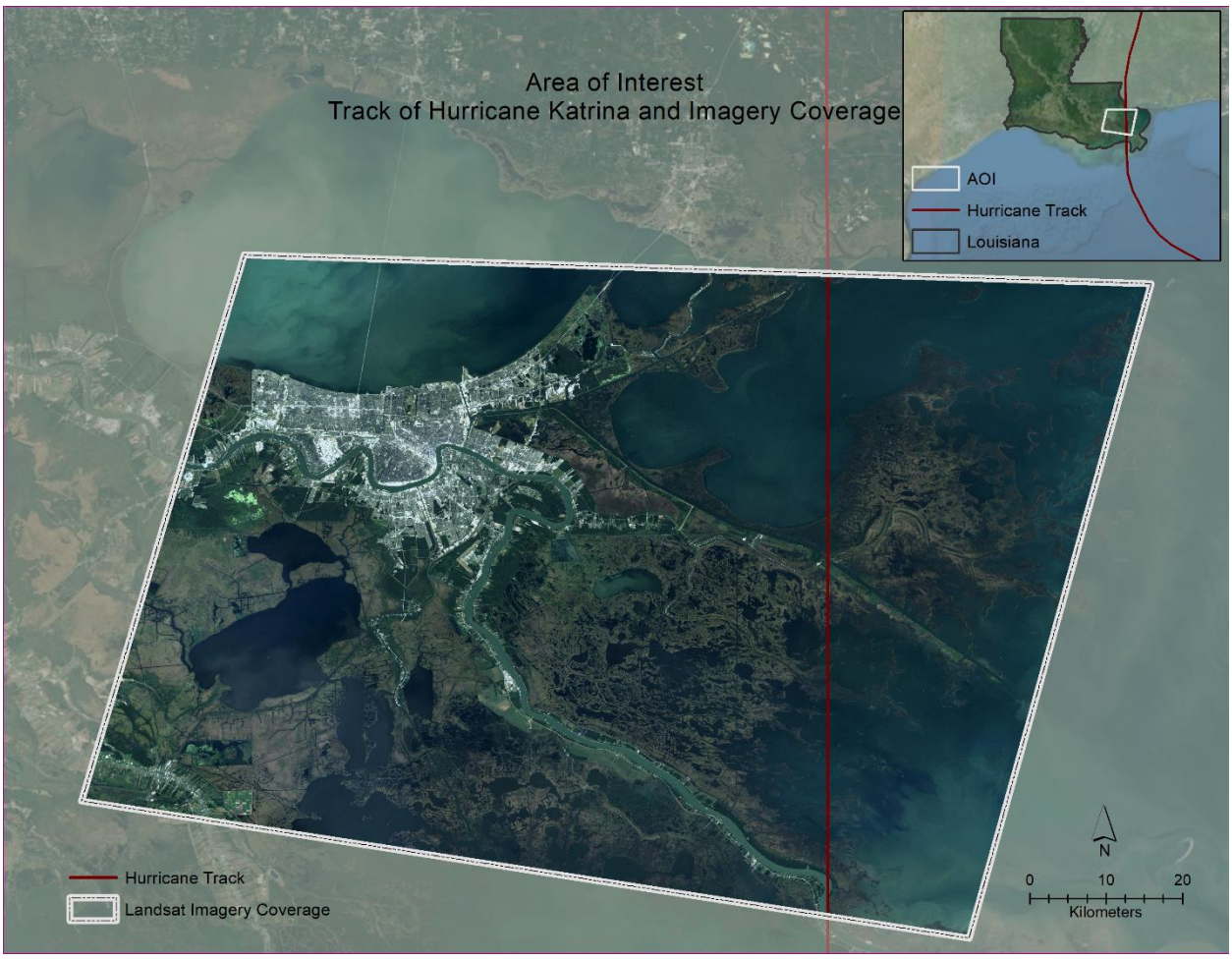

Figure 2. Map of study area, imagery coverage, and Hurricane Katrina track through the AOI.

In previous research, assessments of Hurricane Katrina land cover changes use multiple methodologies [Rodgers *et al.,* 2009; Reif *et al.,* 2011; Evans *et al.,* 2012]. One article examined NDVI changes from Hurricane Katrina, assessing rebound over one year, within the Weeks Bay Reserve in Alabama [Rodgers *et al.,* 2009]. Rodgers' analysis proved that the Normalized Difference Vegetation Index (NDVI) is an important tool for change detection, and this study replicates portions of that methodology. Another study used hyperspectral imagery and LIDAR data to analyze land cover changes over a three-year period after Hurricane Katrina's landfall,

[Reif *et al.,* 2011]. Of note, the Reif study did not use data prior to Hurricane Katrina's landfall as a control for the change analysis. Another study utilized 3-band Landsat derived imagery to perform unsupervised (ISODATA) land cover classification (LCC) along the Mississippi Gulf Coast [Evans *et al.,* 2012]. Evans' analysis focused on imagery prior to Hurricane Katrina (2005) compared to imagery soon after Hurricane Katrina (2006) and performed simple change detection as a percentage of land area.

Hurricane Katrina is a representative event that defines morphological changes to vegetation and land cover that occurs because of traumatic natural disasters. Additionally, due to the time that has elapsed since the disaster occurred, further analysis will assess recovery.

1. Objectives

After a thorough review of existing literature, no published analysis combines land cover classification (LCC) and NDVI to quantify and qualify land cover rebound after 15 years of Katrina's landfall. The goal of this paper is to accomplish this analysis. This study uses Landsat 5 and Landsat 8 surface reflectance tier one scenes from southeastern Louisiana to create multi-temporal NDVI, which will assist in highly accurate LCC maps, created within Google Earth Engine (GEE). This analysis employs these methodologies as a means of classifying and quantifying vegetation changes. Put simply, this paper aims to answer the questions:

- How did Hurricane Katrina change the landscape of southeastern Louisiana?
- How has the landscape recovered now that 15 years have passed since the disaster?

II. METHODS

The analysis began by gathering imagery in GEE for three time-periods: prior to hurricane landfall, immediately after hurricane landfall, and 15 years after hurricane landfall [Gorelick *et al.,* 2017]. This allows for a multi-temporal approach, assessing immediate damage, as well as rebound of the wetland ecosystem. JavaScript coding, in Google Earth Engine (GEE), reduced the Landsat image using a cloud sort method to select the least cloudy image for each time-period (Table 1).

Table 1. Imagery dates and satellite sensors.

Reference	Satellite Sensor	Spatial Resolution	Image Date
LS1	Landsat 5 TM	30 meters	10/04/2003
LS2	Landsat 5 TM	30 meters	10/25/2005
LS3	Landsat 8 OLI	30 meters	10/02/2020

Each full resolution Landsat image covered the full extent of the AOI (Figure 2). Time-period one and time-period two images (LS1 and LS2) are from the Landsat 5 thematic mapper satellite

sensor, and time-period three (LS3) is from the Landsat 8 Operational Land Imager. The near infrared band is especially important in this study due to the value it provides with regard to vegetation health and biomass studies. Although the spectral, spatial and radiometric properties of different Landsat sensors are very similar, there are small differences that can have significant impacts on results. The band with the greatest root mean square deviation (RMSD) in surface reflectance between the two satellites is the NIR band (Figure 3) [Roy *et al.,* 2016].

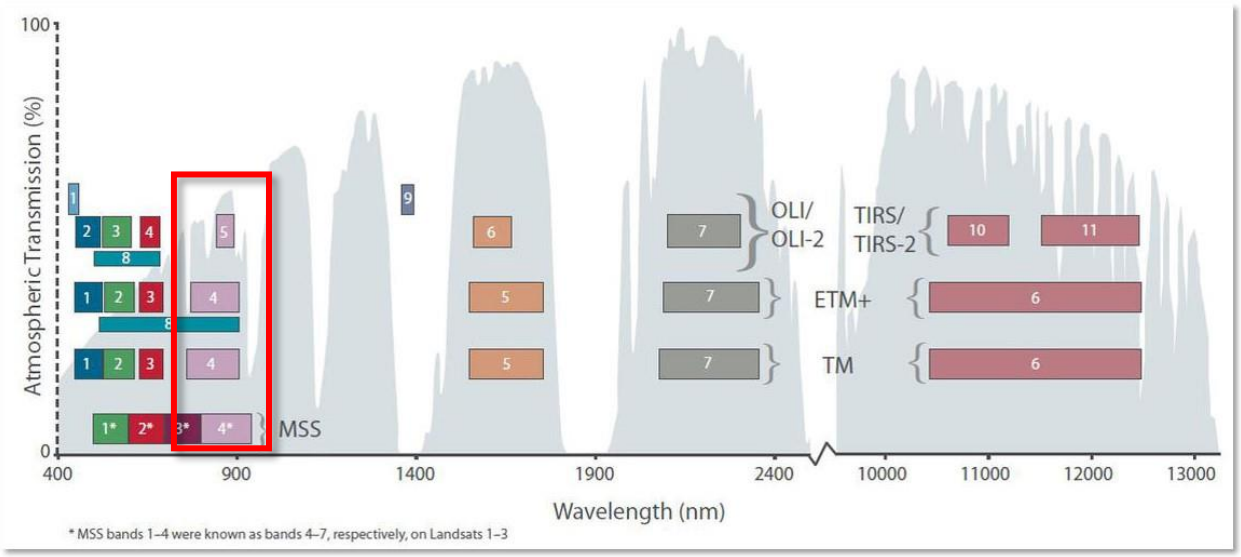

Figure 3. United States Geological Survey graph of spectral response for Landsat sensors. The red box indicates the wavelengths captured by the near infrared band.

For this reason, it is important to employ harmonization techniques. Harmonization is a spectral transformation function that standardizes the pixel spectral response, thereby minimizing the constraints of different spectral, spatial and radiometric properties, so that images from different sensors can be accurately compared [Roy *et al.,* 2016]. JavaScript coding within GEE applies established radiometric calibration coefficients to each image. This achieves the necessary harmonization for accurate comparative analysis [Chander *et al.,* 2009].

NDVI data reliably quantifies vegetation change, biomass and leaf area index, with success in many coastal environments, [Rodgers *et al.,* 2009]. The NDVI was calculated with the equation NDVI = (NIR – Red)/(NIR + Red) where near infrared (NIR) is the near infrared TM band 4 or OLI band 5, and Red is the visible red TM band 3 or OLI band 4, [Dong *et al.,* 2014], [Markogianni *et al.,* 2013]. The NIR band corresponds to the long wavelength shoulder of the chlorophyll red-edge, and the red band corresponds to the wavelengths with the maximum chlorophyll absorption, [Jensen, 2005]. This means that high NDVI values are indicative of denser live green vegetation.

Further analysis was needed in order to quantify the change that had taken place. In order to accomplish this it was necessary to change the image from floating point to integer by utilizing the equation ((NDVI*0.5)+0.5)*100. This changed the values so that the image no longer ranged from -1 to 1 but instead from 0 to 100. It is necessary to have all positive values so that proper raster subtraction can take place. The resulting images were then subtracted using formula $\Delta NDVI=NDVI_2-NDVI_1$, where $NDVI_2$ is the most recent date, and $NDVI_1$ is the earlier date, in order to assess the multi-temporal changes in NDVI, [Mancino *et al.,* 2014]. The resulting layers have positive values corresponding to increases in NDVI, and negative values corresponding to decrease in NDVI.

The supervised classification methodology chosen for this study is Random Forest (RF) Classification. Through iterative analysis on the training dataset of target classes, the RF supervised classification method has often proven successful, particularly for wetland and mangrove classification [Tian *et al.,* 2016]. Additionally, research finds that RF classifiers outperform other methods such as decision tree, classification and regression tree, maximum likelihood and support vector machine, [Na *et al.,* 2010; Rodriguez-Galiano *et al.,* 2012; Tian *et al.,* 2016; Wang *et al.,* 2019].

The fusion of remote sensing data, such as medium resolution Landsat imagery, band ratios such as NDVI, and supervised LCC methods such as RF, combine to result in improved classification accuracy, [Jia *et al.,* 2014].

The analyst trained the RF classifier in GEE for each time-period, and completed multiple classification iterations until the results met visual satisfaction. Next, the analyst downloaded the results locally and imported into ArcGIS Pro for a thorough accuracy assessment. A combination approach using stratified random and equalized stratified random assessment points ensured an appropriate point spread throughout the dataset while maintaining a minimum number of 50 points per class [Ramezan, Warner & Maxwell, 2019]. The analyst assessed each point by viewing the Landsat imagery and recording the class at each point without view of the LCC. This ensured there was no bias in the ground truth field. ArcGIS Pro tools computed the confusion matrix for each time-period (Tables 2-4).

The error matrix has been standard practice for measuring the accuracy of Landsat imagery derived maps since the 1980s [Congalton, 2001]. The Kappa coefficient is a measure of statistical significance that answers the question of whether a map is significantly better than random chance [Congalton, 2001]. Kappa values better than 0.80 represent strong agreement [Congalton, 2001].

2003 Confusion Matrix									
Class Name	**Wetlands**	**Other Vegetation**	**High Density Urban**	**Water**	**Bare Earth**	**Low/Medium Density Urban**	**Total**	**User Accuracy**	**Kappa Coefficient**
Wetlands	238	8	0	6	2	4	258	0.922481	0
Other Vegetation	13	93	1	0	0	0	107	0.869159	0
High Density Urban	0	0	60	0	0	0	60	1	0
Water	1	0	0	352	0	0	353	0.997167	0
Bare Earth	2	1	1	1	42	13	60	0.7	0
Low/Medium Density Urban	3	3	2	0	1	61	70	0.871429	0
Total	257	105	64	359	45	78	908	0	0
Producer Accuracy	0.92607	0.885714	0.9375	0.980501	0.933333	0.782051	0	0.931718	0
Kappa Coefficient	0	0	0	0	0	0	0	0	0.907438

Table 2. Accuracy assessment confusion matrix, 2003

In the 2003 imagery, some classes performed better than others, but the overall accuracy was still a high 93%, and the Kappa coefficient was just over 90%.

2005 Confusion Matrix									
	Wetlands	**Other Vegetation**	**High Density Urban**	**Water**	**Bare Earth**	**Low/Medium Density Urban**	**Total**	**User Accuracy**	**Kappa Coefficient**
Wetlands	233	9	0	10	4	5	261	0.89272	0
Other Vegetation	17	68	0	0	1	1	87	0.781609	0
High Density Urban	0	0	52	1	2	5	60	0.866667	0
Water	1	0	0	364	0	0	365	0.99726	0
Bare Earth	4	3	1	1	55	3	67	0.820896	0
Low/Medium Density Urban	3	5	0	0	10	46	64	0.71875	0
Total	258	85	53	376	72	60	904	0	0
Producer Accuracy	0.903101	0.8	0.981132	0.968085	0.763889	0.766667	0	0.904867	0
Kappa Coefficient	0	0	0	0	0	0	0	0	0.868985

Table 3. Accuracy assessment confusion matrix, 2005

The imagery from 2005 had some minor cloudiness that did affect the classifier performance. Still the overall accuracy was a reasonable 90% and the kappa coefficient was nearly 87%. This is a more than satisfactory classification result [Congalton, 2001].

2020 Confusion Matrix									
Class Name	Wetlands	Other Vegetation	High Density Urban	Water	Bare Earth	Low/Medium Density Urban	Total	User Accuracy	Kappa Coefficient
Wetlands	222	5	0	3	6	2	238	0.932773	0
Other Vegetation	23	79	0	0	1	1	104	0.759615	0
High Density Urban	0	0	54	1	0	5	60	0.9	0
Water	1	0	0	375	0	0	376	0.99734	0
Bare Earth	4	3	5	5	39	4	60	0.65	0
Low/Medium Density Urban	0	7	3	0	4	57	71	0.802817	0
Total	250	94	62	384	50	69	909	0	0
Producer Accuracy	0.888	0.840426	0.870968	0.976563	0.78	0.826087	0	0.908691	0
Kappa Coefficient	0	0	0	0	0	0	0	0	0.874465

Table 4. Accuracy assessment confusion matrix, 2020

In 2020 imagery, the overall accuracy was again a satisfactory 90% and the kappa coefficient was just over 87%. The classifier did struggle to achieve these results due to the sun glint in the image, and required multiple iterations to achieve these results.

Once the LCC outputs met accuracy standards, as confirmed by the accuracy assessment metrics, the change detection process continued within GEE. Changes were assessed between LCC outputs from time-period one (LCC1) and time-period two (LCC2), between LCC2 and time-period three (LCC3), and finally between LCC1 and LCC3 (Figure 3).

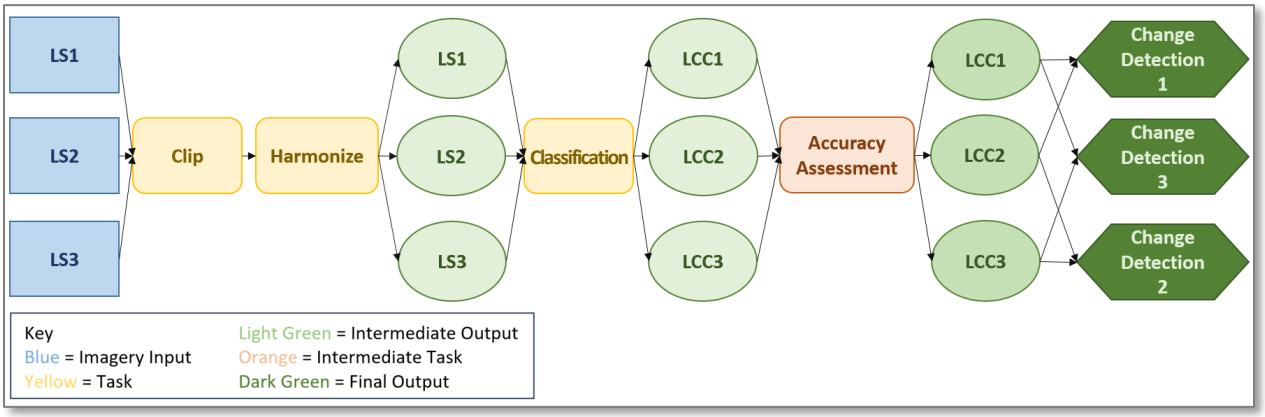

Figure 3. Change detection workflow diagram

III. RESULTS

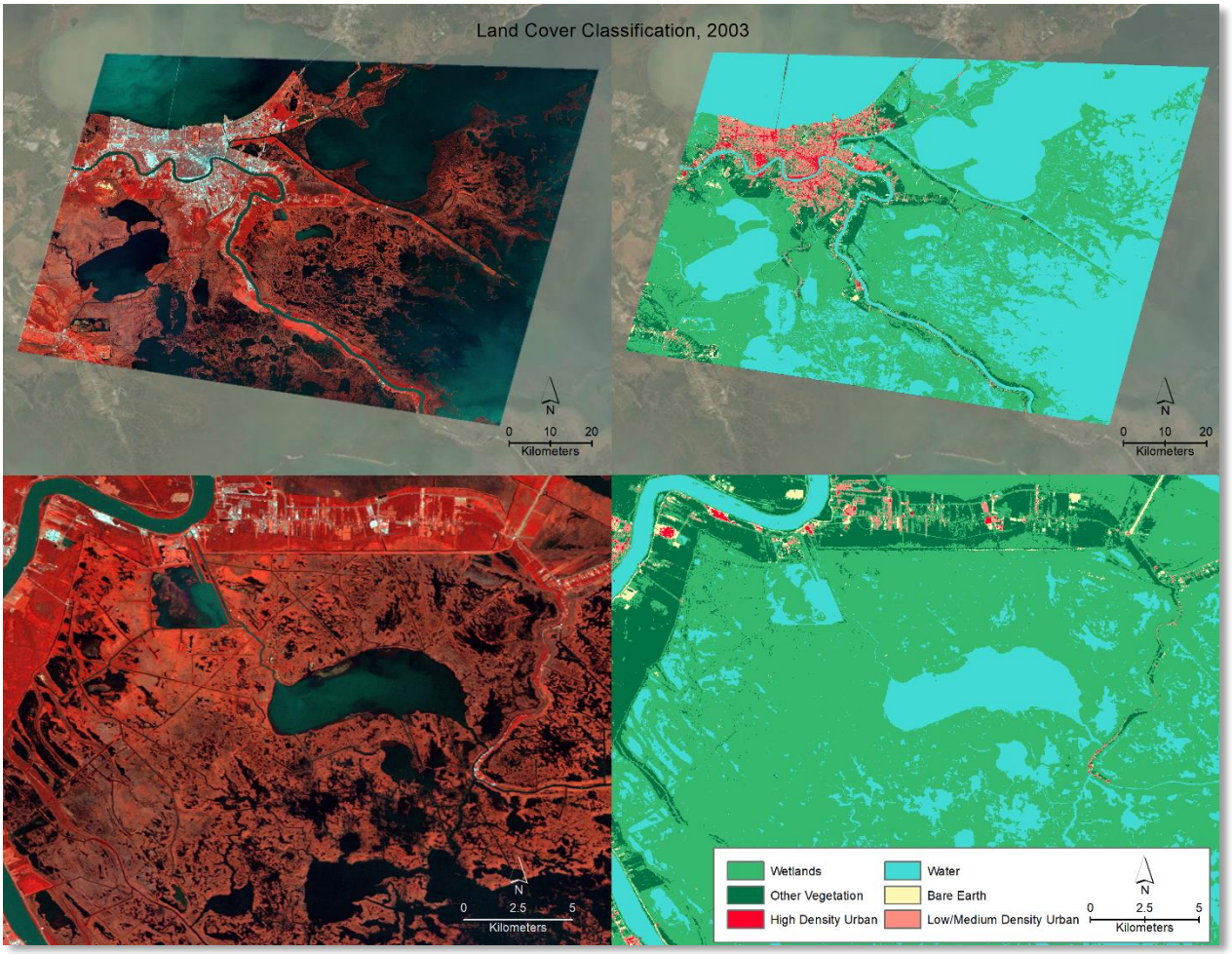

Figure 4. False color satellite imagery and LCC maps from time-period one (2003).

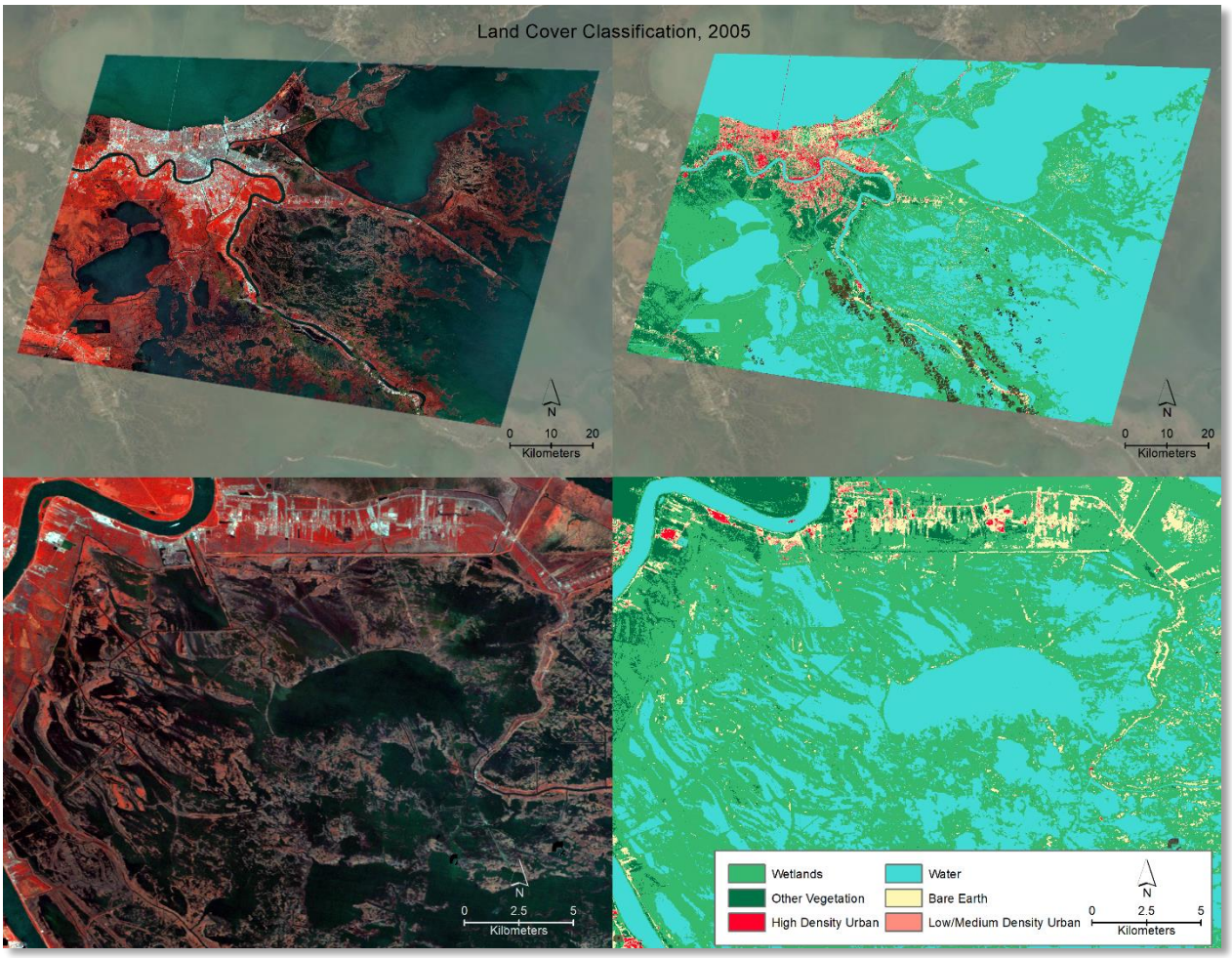

Figure 5. False color satellite imagery and LCC maps from time-period two (2005).

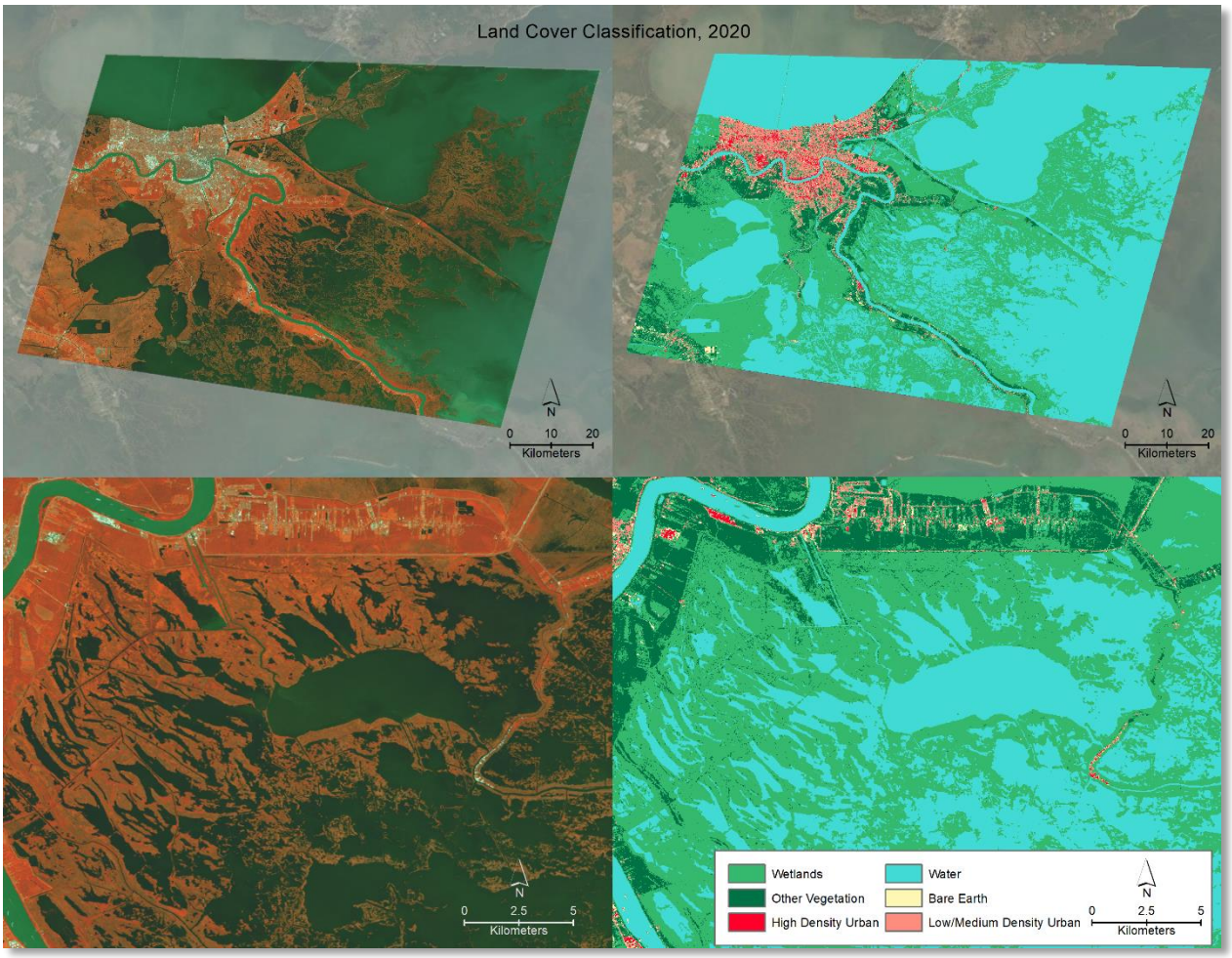

Figure 6. False color satellite imagery and LCC maps from time-period three (2020).

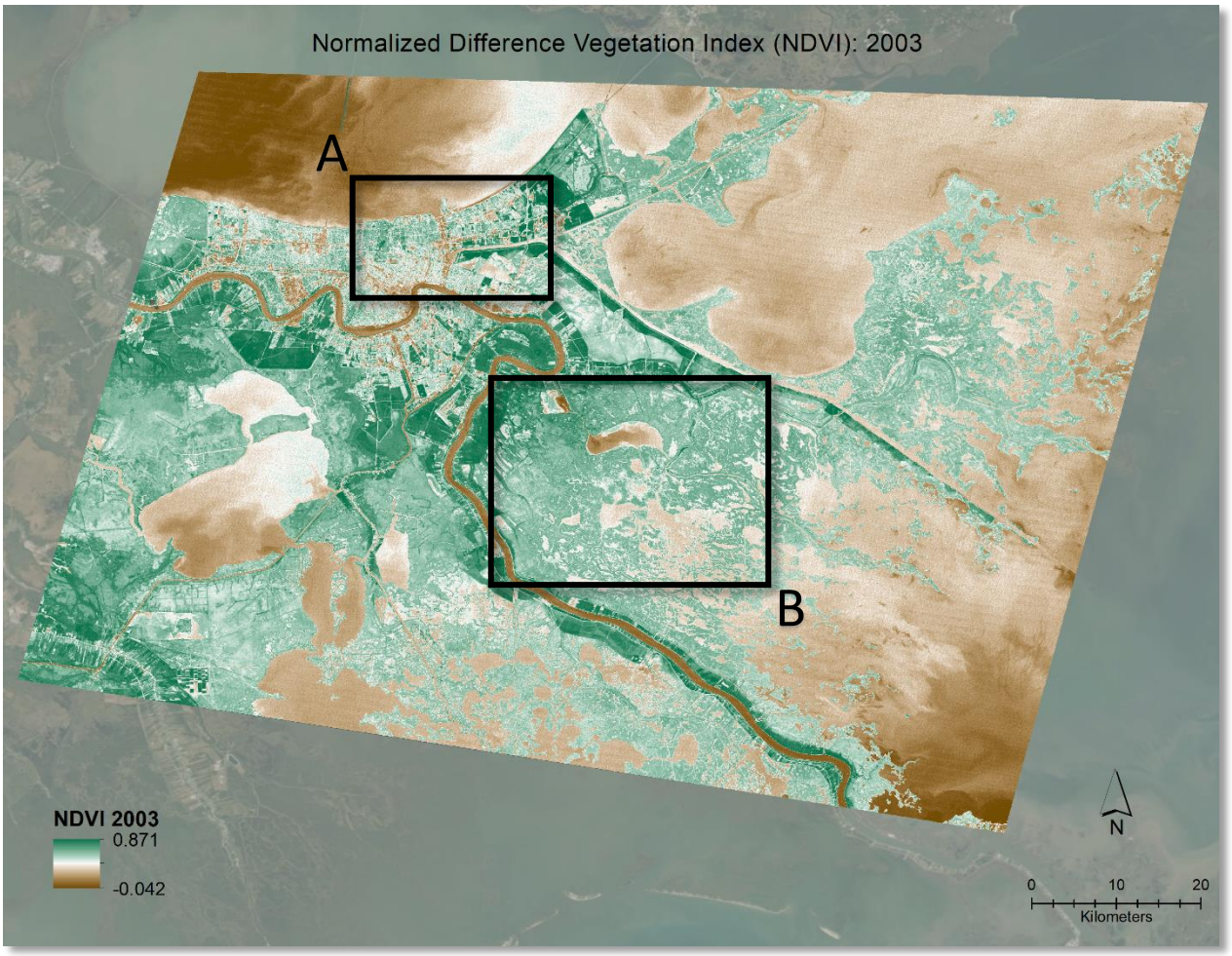

Figure 7. NDVI, 2003

Very healthy vegetation (darker greens) is apparent in the suburban areas south of Lake Pontchartrain as well as in the dense wetland areas of eastern Plaquemines Parish.

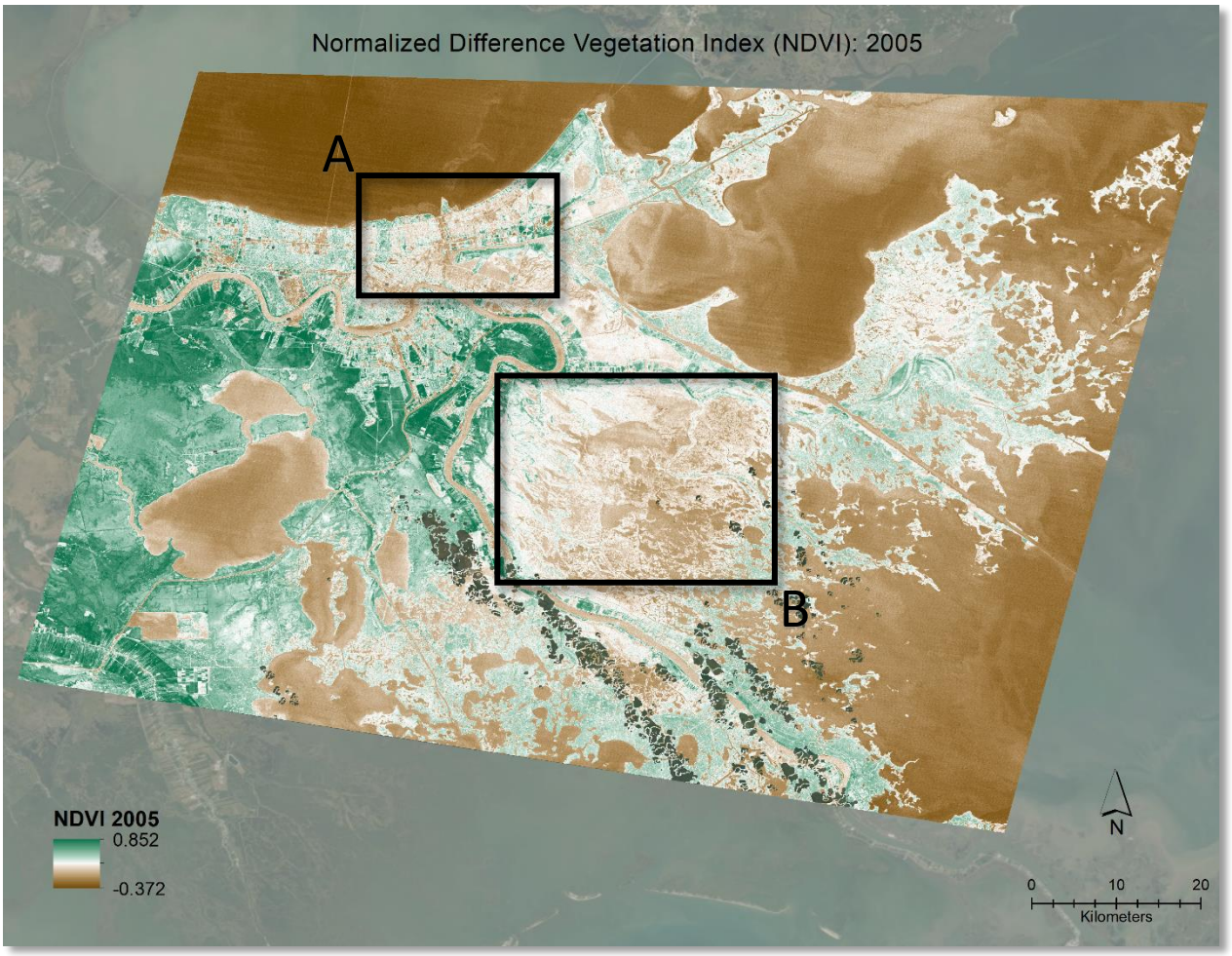

Figure 8. NDVI, 2005

After Hurricane Katrina passed through the area, the previously healthy vegetation turned to either unhealthy or even non-existent vegetation, indicated by the more neutral to brown colors.

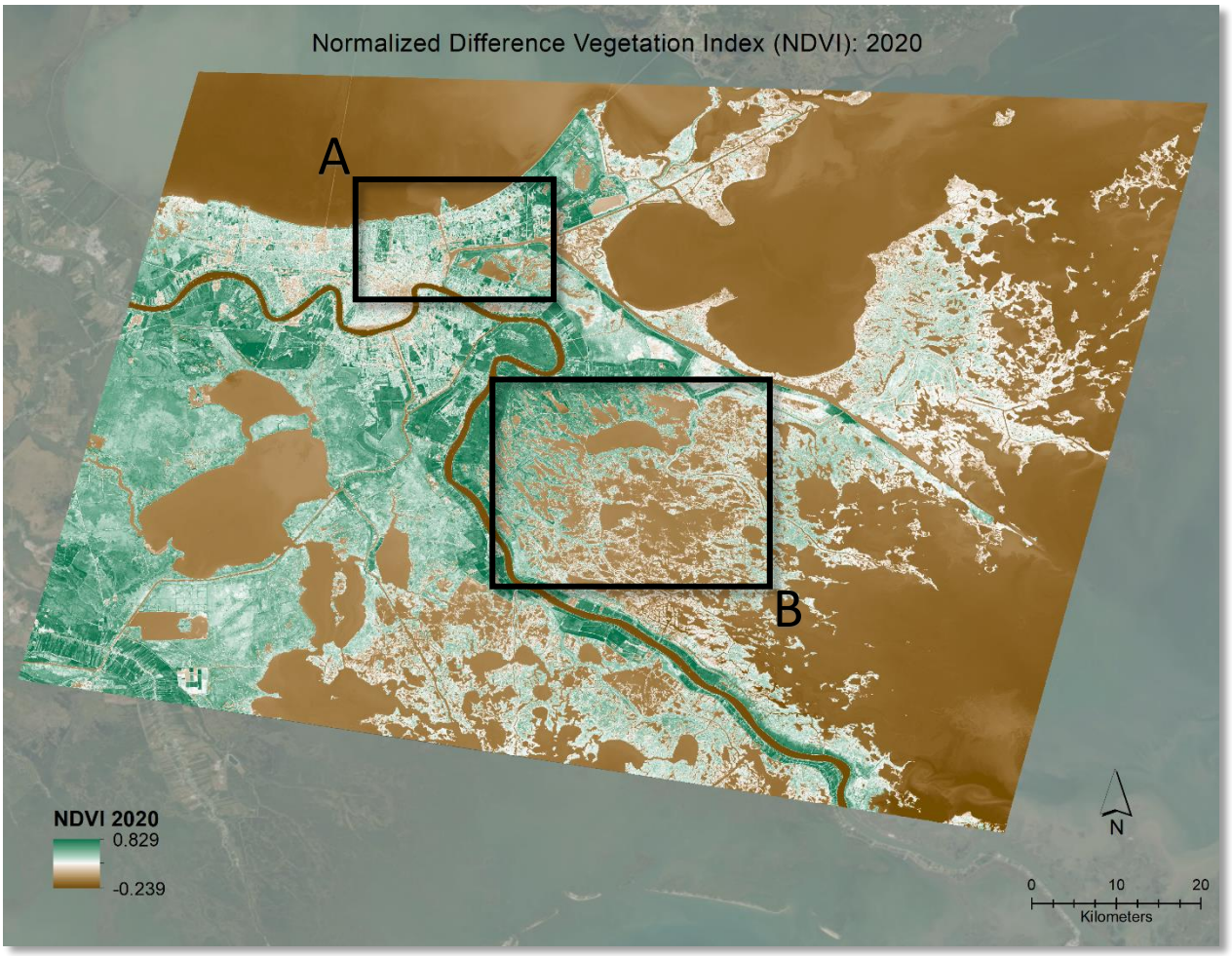

Figure 9. NDVI, 2020

The greenness, related to vegetation occurrence, increased in the boxed areas indicating a return of healthy vegetation. Still, it is visually apparent that the full extent of healthy wetlands has not returned.

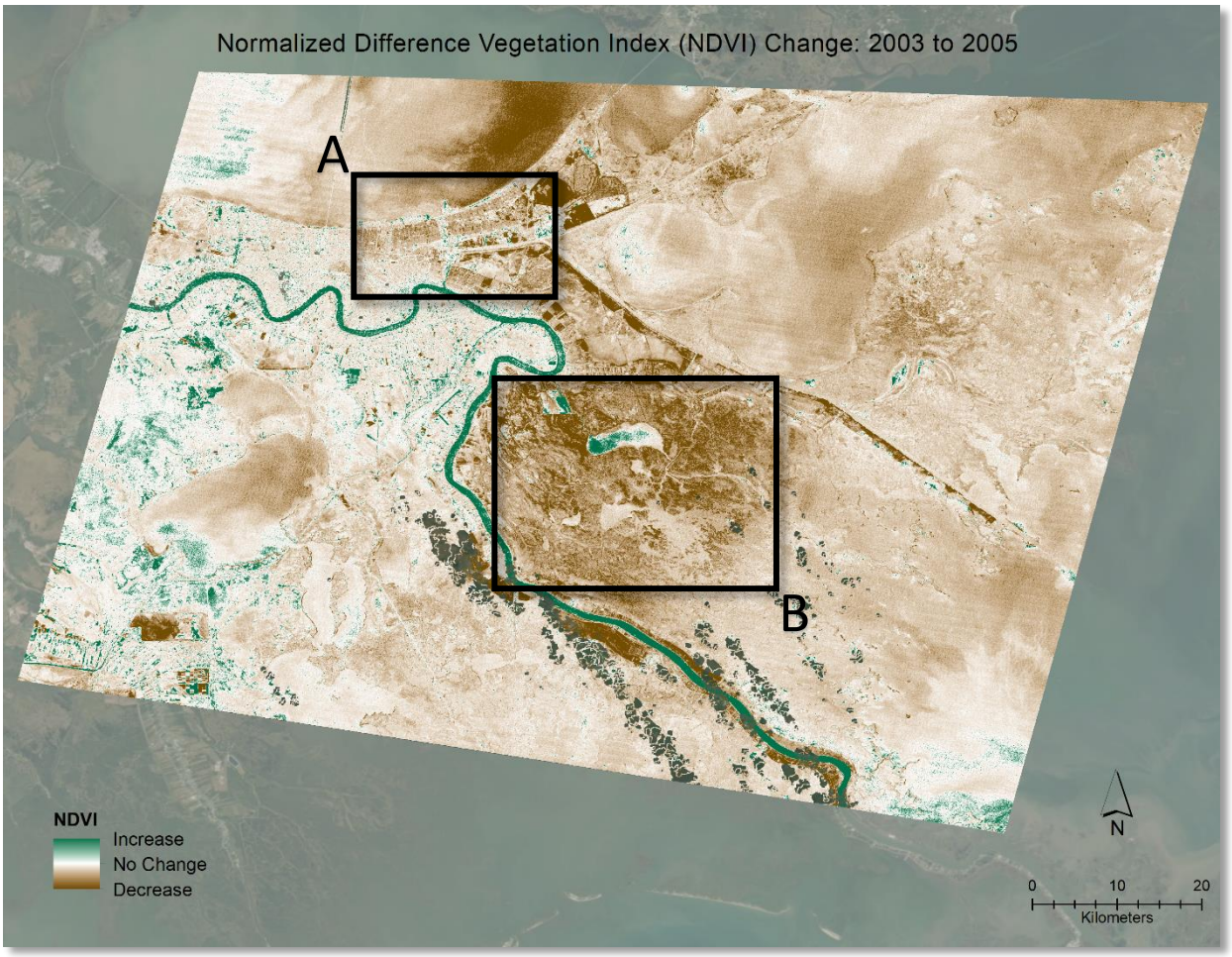

Figure 10. NDVI Change, 2003 to 2005

From 2003 to 2005, the NDVI change detection results showed the expected drastic reduction in NDVI over a large part of the AOI. This decrease is most notable in the dense wetlands found toward the center of the AOI. It is also interesting to note the decrease of NDVI in the dense urban and suburban areas south of Lake Pontchartrain. The storm surge inundation and subsequent levee breaks caused extreme flooding in this area, inundating homes and destroying much of the vegetation.

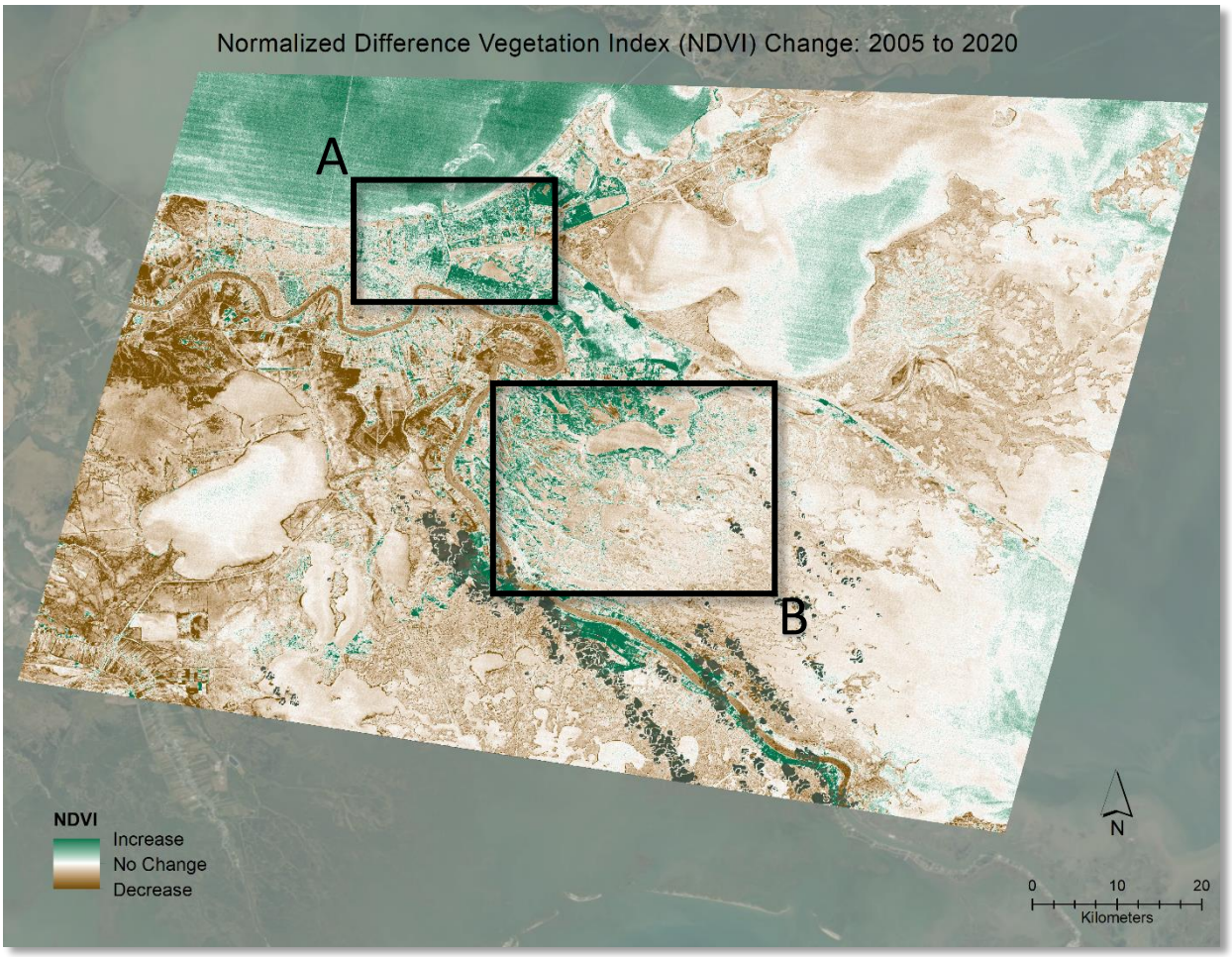

Figure 11. NDVI Change, 2005 to 2020

From 2005 to 2020, there was an increase in NDVI in the wetland areas of northeast Plaquemines parish as well as noticeable increase within the urban and suburban areas along the south shore of Lake Pontchartrain. Some areas of previously destroyed vegetation regrew in the 15 years following the hurricane, especially along the Mississippi River.

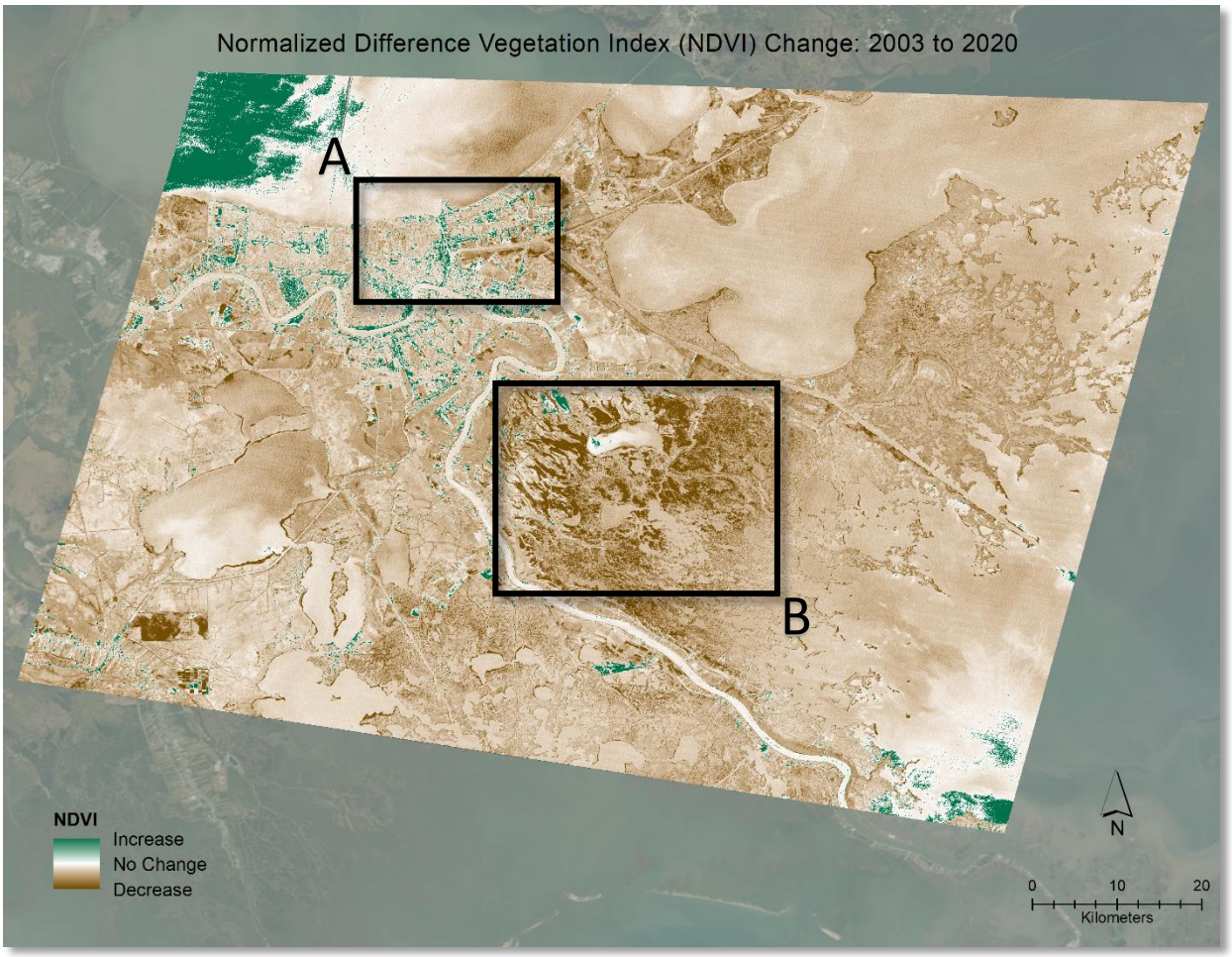

Figure 12. NDVI Change, 2003 to 2020

Overall, there was a notable decline in NDVI from 2003 to 2020, especially in the dense wetland areas of northeast Plaquemines parish. Although some areas appear to have recovered to pre-Katrina levels of vegetation health, a large area of vegetation remains destroyed.

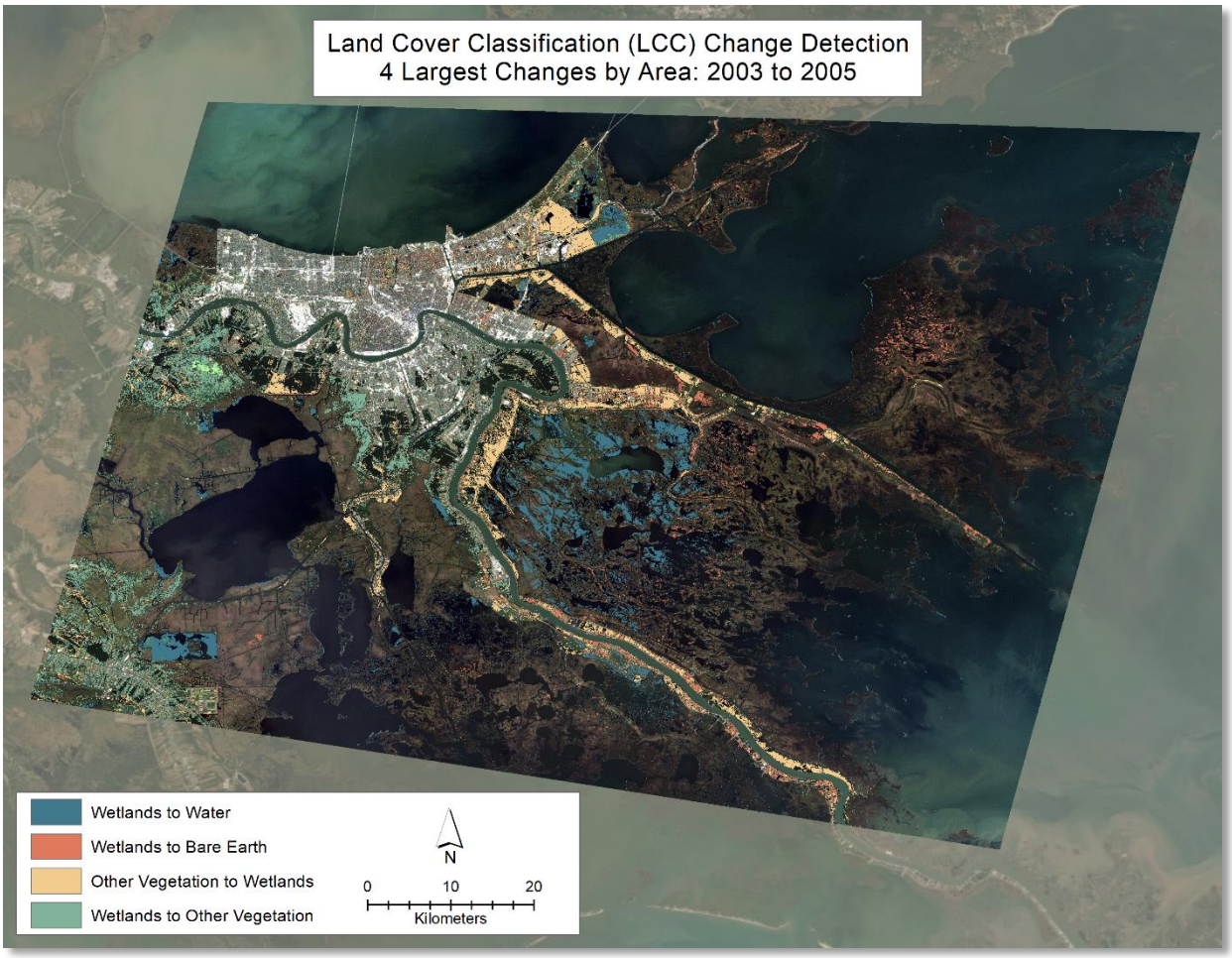

Figure 13. Top four class changes, 2003 to 2005

Classification 2003	Classification 2005	Area (Sq. Km.)
Wetlands	Water	195.9174
Other Vegetation	Wetlands	186.426
Wetlands	Other Vegetation	169.5762
Wetlands	Bare Earth	94.3821

Table 5: LCC Change, 2003 to 2005

From 2003 to 2005, there was a large loss of wetland area. These areas changed to water, other vegetation and bare earth. The most significant change was from wetlands to water, with 195 square kilometers of wetland loss.

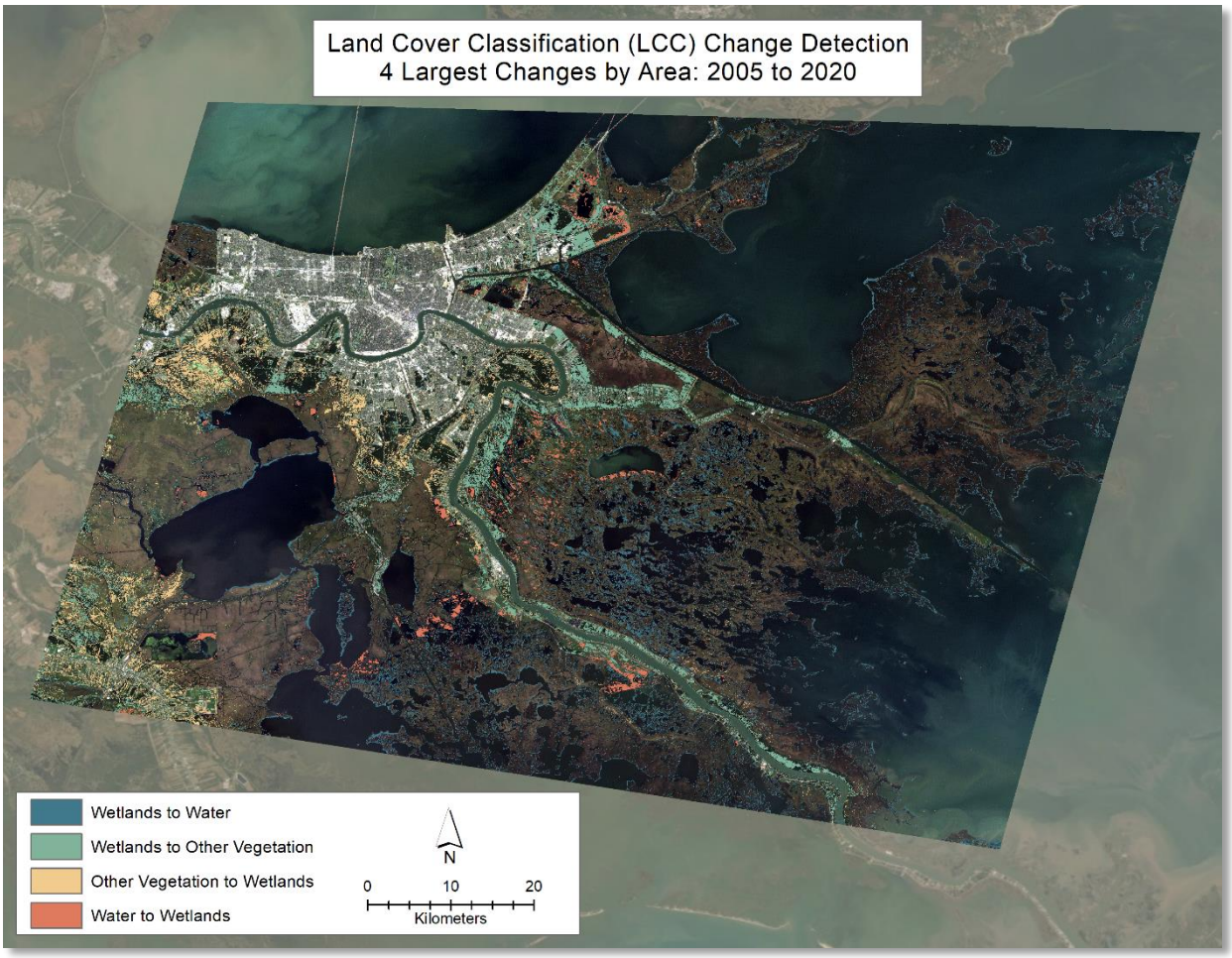

Figure 14. Top four class changes, 2005 to 2020

Classification 2005	Classification 2020	Area (Sq. Km.)
Wetlands	Water	295.2738
Wetlands	Other Vegetation	215.5707
Other Vegetation	Wetlands	149.1561
Water	Wetlands	83.4615

Table 6: LCC Change, 2005 to 2020

From 2005 to 2020, wetlands did show a rebound, and the other vegetation and water class changed to the wetland classification. Once again, the most significant change was from wetlands to water, with 295 square kilometers of wetland loss.

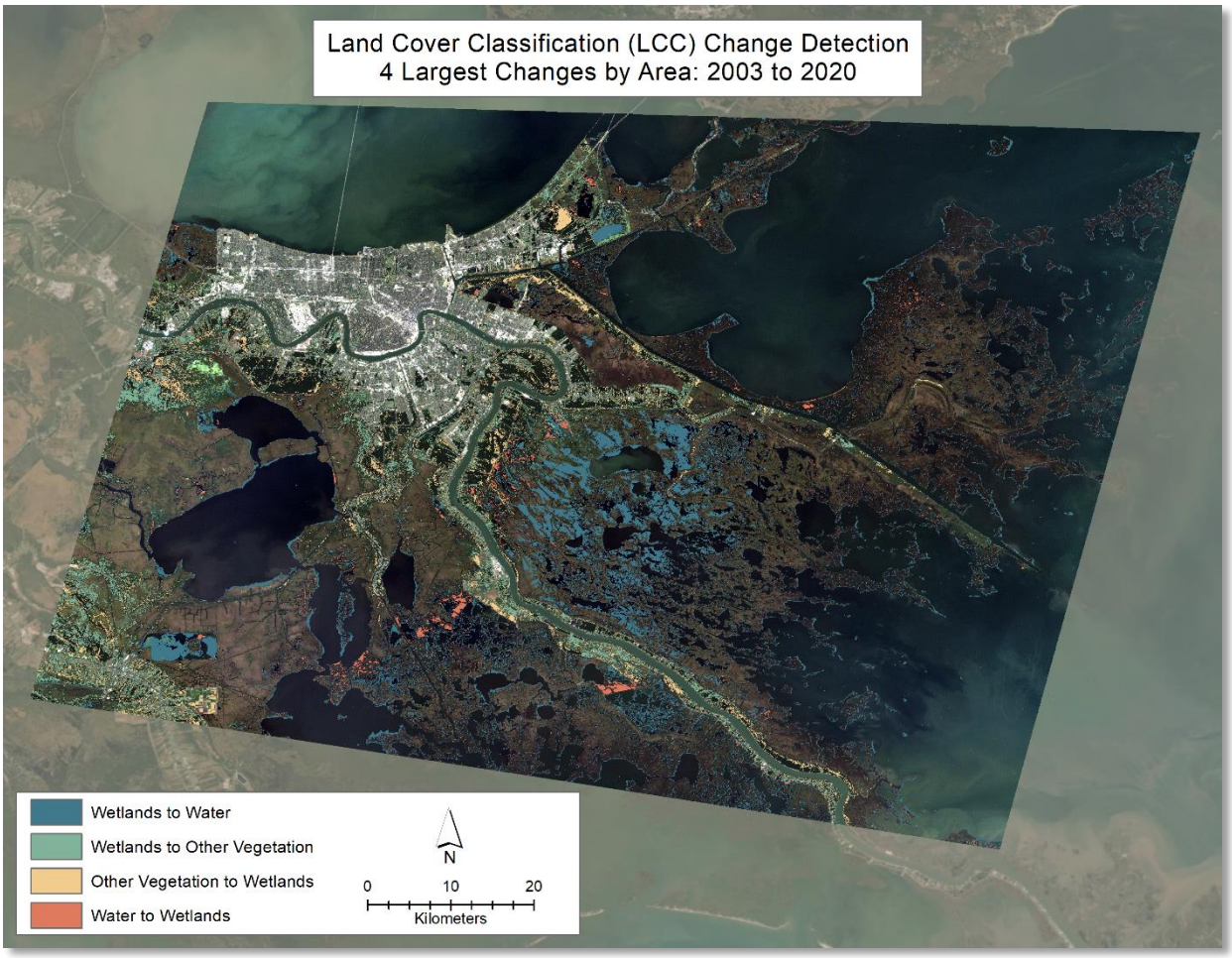

Figure 15. Top four class changes, 2003 to 2020

Classification 2003	Classification 2020	Area (Sq. Km.)
Wetlands	Water	420.4854
Wetlands	Other Vegetation	178.8804
Other Vegetation	Wetlands	127.8252
Water	Wetlands	60.0705

Table 7: LCC Change, 2003 to 2020

From 2003 to 2020, there has been a prominent change. By far the most significant change is from wetlands to water, with over 420 square kilometers of wetland loss in this time-period. This indicates that a large area of wetlands that existed 2003 were destroyed, and can likely be considered a permanent loss.

IV. DISCUSSION

Decrease in NDVI was especially profound in the urban areas south of Lake Pontchartrain, and in the wetland areas of northeast Plaquemines parish. The overall result of this research is that marsh vegetation was lost, most likely due to the catastrophic storm surge and resulting saltwater inundation from Hurricane Katrina. Increased rip currents, wave action, and wind likely caused this widespread destruction of an already fragile landscape [Shirley, 2012]. Since 2003, the results indicate a loss of over 420 square kilometers of wetlands to the water class. This wetland loss is ongoing, and will be permanently lost without proper mitigation efforts. This wetland loss is certainly an urgent matter due to the devastating effect on local ecology, including the many threatened and endangered wildlife and marine species that call this area home. In addition to the local ecology, mitigation of wetland loss decreases hurricane impacts on coastal communities since wetlands buffer wind, waves, and surge action.

1. Future Work

This analysis will continue for every year from 2003 through 2020 to trace the exact timing of the major changes in land cover, and to discover a cause for the continuing wetland loss found in this analysis. This analysis will include other disasters, such as Hurricane Isaac and the Deep Water Horizons oil spill, that are likely to have had an impact on the wetlands in the area.

V. ACKNOWLEDGEMENTS

The author would like to thank and acknowledge Dr. Douglas Miller for his expertise and advisement that was much appreciated.

VI. LITERATURE CITED

1. Chander, Gyanesh, Brian L. Markham, Dennis L. Helder (2009) Summary of current radiometric calibration coefficients for Landsat MSS, TM, ETM+, and EO-1 ALI sensors. *Remote Sensing of Environment*, 113(5): 893-903.
2. Congalton, Russell (2001) Accuracy assessment and validation of remotely sensed and other spatial information. *International Journal of Wildland Fire,* 10(4): 321-328.
3. Costanza, Robert, Octavio Perez-Maqueo, M. Luisa Martinez, Paul Sutton, Sharolyn Anderson, and Kenneth Mulder (2008) The Value of Coastal Wetlands for Hurricane Protection. *Ambio*, 37(4): 241-248.
4. Dong, Z., Z. Wang, D. Liu, K. Song, L. Li, M. Jia, and Z. Ding (2014), Mapping Wetland Areas Using Landsat-Derived NDVI and LSWI: A Case Study of West Songnen Plain, Northeast China. *Journal of the Indian Society of Remote Sensing,* 42(3), 569-577.

5. Evans E.D., Anjaneyulu Y., Tchnouwou P.B. (2012) Effects of Hurricane Katrina on Land Cover Within the Grand Bay National Estuarine Research Reserve in Mississippi, USA. *Environmental and Food Safety and Security for South-East Europe and Ukraine. NATO Science for Peace and Security Series C: Environmental Security*, 122(1): 173-188.
6. Ghandi, M., S. Parthiban, N. Thummalu, and A. Christy (2015) NDVI: Vegetation Change Detection Using Remote Sensing and GIS – A Case Study of Vellore District. *Procedia Computer Science*, 57(1): 1199-1210.
7. Gorelick, N., Hancher, M., Dixon, M., Ilyushchenko, S., Thau, D., & Moore, R. (2017) Google Earth Engine: Planetary-scale geospatial analysis for everyone. *Remote Sensing of Environment*, 202(1): 18-27.
8. Jia, K., S. Liang, L. Zhang, X. Wei, Y. Yao, and X. Xie (2014), Forest Cover Classification using Landsat ETM+ Data and Time Series MODIS NDVI Data. *International Journal of Applied Earth Observation and Geoinformation*, 33(1): 32-38.
9. Knabb, R. D., J. R. Rhome, and D. P. Brown (2005), Tropical Cyclone Report: Hurricane Katrina, 23-30 August 2005. *National Oceanic and Atmospheric Administrations, National Hurricane Center, Miami, Florida*.
10. Lawrence, Rick and Andrea Wright (2001), Rule-Based Classification Systems Using Classification and regression Tree (CART) Analysis. *Photogrammetric Engineering & Remote Sensing*. 67(10): 1137-1142.
11. Li, X., Yu, L., Xu, Y. (2016), Ten years after Hurricane Katrina: monitoring recovery in New Orleans and the surrounding areas using remote sensing. *Science Bulletin*, 61(18): 1460–1470.
12. Mancino, G., A. Nole, F. Ripullone, and A. Ferrara (2014), Landsat TM Imagery and NDVI Differencing to Detect Vegetation Change: Assessing Natural Forest Expansion in Basilicata, Southern Italy. *iForest,* 7, 75-84.
13. Markogianni, V., E. Dimitriou, and D. P. Kalivas (2013), Land-Use and Vegetation Change Detection in Plastira Artificial Lake Catchment (Greece) by using Remote-Sensing and GIS Techniques. *International Journal of Remote Sensing,* 34(4), 1265-1281.
14. Morton, Robert and John Barras (2011), Hurricane Impacts on Coastal Wetlands: A Half-Century Record of Storm-Generated Features from Southern Louisiana. *Journal of Coastal Research*, 27(6A): 27-43.
15. Na, X., S. Zhang, X. Li, H. Yu, and C. Liu (2010), Improved Land Cover Mapping using Random Forests Combined with Landsat Thematic Mapper Imagery and Ancillary Geographic Data. *Photogrammetric Engineering & Remote Sensing*, 76(7): 833-840.
16. National Wildlife Foundation. Https://www.nwf.org/Wildlife/Wild-Places/Mississippi-River-Delta.aspx
17. Pantaleoni, E., R.H. Wynne, J.M. Galbraith, and J.B. Campbell (2009), Mapping wetlands using ASTER data: a comparison between classification trees and logistic regression. *International Journal of Remote Sensing*, 30(13): 3423-3440.

18. Ramezan, Christopher, Timothy Warner and Aaron Maxwell (2019) Evaluation of Sampling and Cross-Validation Tuning Strategies for Regional-Scale Machine Learning Classification. *Remote Sensing.* 11(2):185-206.
19. Reif, Molly, Christopher L. Macon, and Jennifer M. Wozencraft (2011), Post-Katrina Land-Cover, Elevation, and Volume Change Assessment along the South Shore of Lake Pontchartrain, Louisiana, U.S.A. *Journal of Coastal Research*, 31(62): 30-39.
20. Rodgers, J. C., A. W. Murrah, and W. H. Cooke (2009), The Impact of Hurricane Katrina on the Coastal Vegetation of the Weeks Bay Reserve, Alabama from NDVI Data. *Estuaries and Coasts*, 32(3): 496-507.
21. Rodriguez-Galiano, V. F., B. Ghimire, J. Rogan, M. Chica-Olmo, and J.P. Rigol-Sanchez (2012), An assessment of the effectiveness of a random forest classifier for land-cover classification. ISPRS Journal of Photogrammetry and Remote Sensing, 67: 93-104.
22. Roy, D.P., V. Kovalskyy, H. K. Zhang, E. F. Vermote, L. Yan, S. S. Kumar, and A. Egorov (2016), Characterization of Landsat-7 to Landsat-8 reflective wavelength and normalized difference vegetation index continuity. *Remote sensing of Environment*, 185(1): 57-70.
23. Shirley, Jolene S. (2012) Louisiana Coastal Wetlands: A Resource at Risk - USGS Fact Sheet. *United States Geological Survey (USGS),* https://pubs.usgs.gov/fs/la-wetlands.
24. Tian, S., X. Zhang, J. Tian, and Q Sun (2016), Random Forest Classification of Wetland Landcovers from Multi-Sensor Data in the Arid Region of Xinjiang, China. *Remote Sensing.* 8(11): 954-967.
25. Wang X, Gao X, Zhang Y, Fei X, Chen Z, Wang J, Zhang Y, Lu X, and Zhao H. (2019) Land-Cover Classification of Coastal Wetlands Using the RF Algorithm for Worldview-2 and Landsat 8 Images. *Remote Sensing.* 11(16):1927.
26. Wenzhao Li, Hesham El-Askary, Mohamed A. Qurban, Jingjing Li, K.P. ManiKandan, Thomas Piechota (2019), Using multi-indices approach to quantify mangrove changes over the Western Arabian Gulf along Saudi Arabia coast. *Ecological Indicators*, 102: 734-745.
27. Wright, C. and A. Gallant (2007), Improved wetland remote sensing in Yellowstone National Park using classification trees to combine TM imagery and ancillary environmental data. *Remote Sensing of Environment*, 107(4): 582-605.